Smart Materials

Advanced Concepts and Research

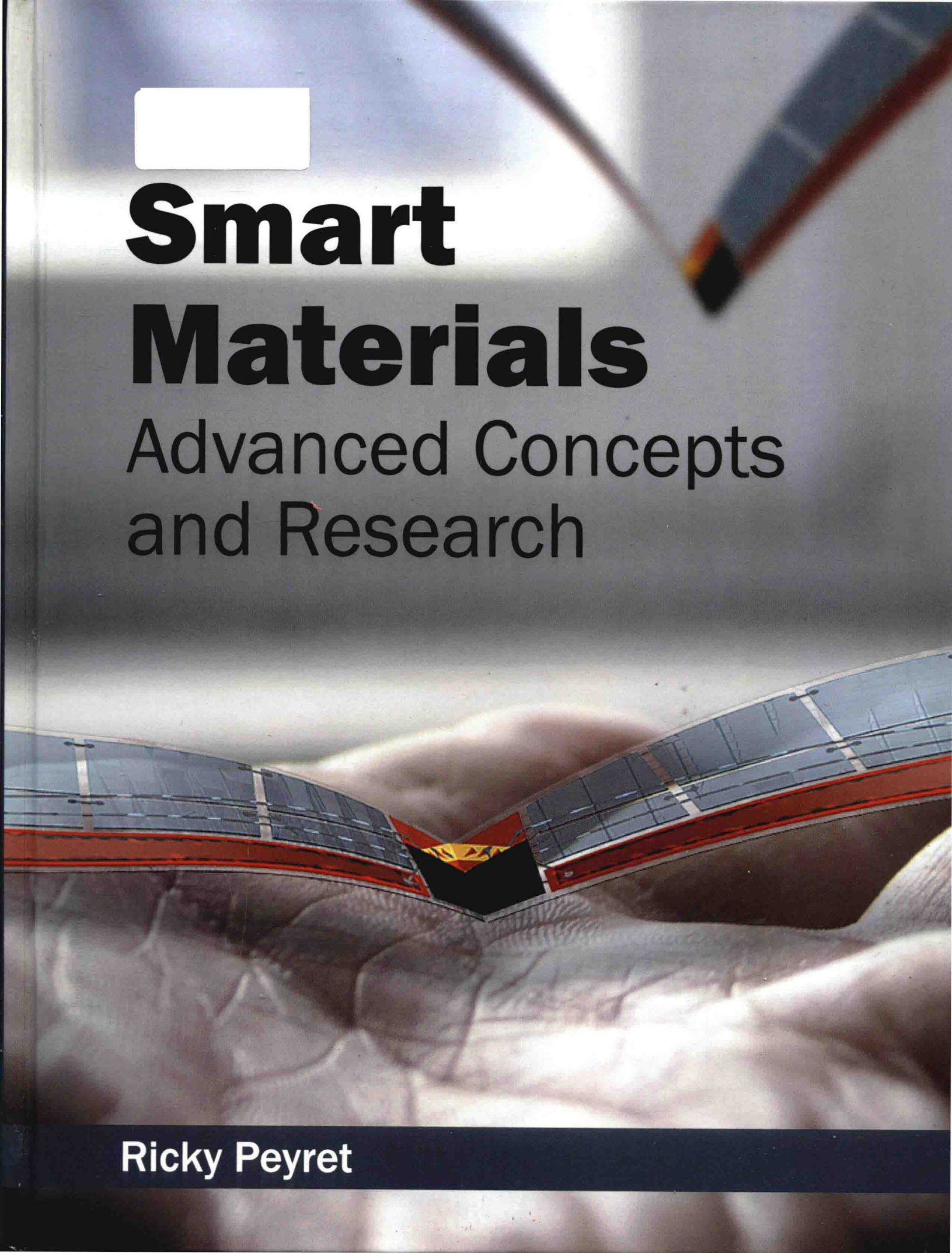

Ricky Peyret

Smart Materials: Advanced Concepts and Research

Edited by **Ricky Peyret**

NY RESEARCH PRESS

New York

Published by NY Research Press,
23 West, 55th Street, Suite 816,
New York, NY 10019, USA
www.nyresearchpress.com

Smart Materials: Advanced Concepts and Research
Edited by Ricky Peyret

International Standard Book Number: 978-1-63238-420-1 (Hardback)

Printed in China.

Smart Materials: Advanced Concepts and Research

Preface

Smart materials are specifically designed materials that can embody one or more characteristics that can be significantly changed in a controlled manner by external stimuli or environment like temperature, moisture, compression, stress, pH level and magnetic and electric fields. This essentially means that smart materials can transform in response to changing conditions in their environment or by the application of other direct external influences. In a nutshell, these materials can change their state and properties. These changes are usually a useful temporary or reversible effect. The induced transformations in the characteristics of the smart material could be in its electrical behaviour, its mechanical properties, optical behaviour or magnetic behaviour. There is now a huge variety of smart materials with various special characteristics that can make a particular material well suited to a particular specific use and the market for such materials is growing day by day. Smart materials are also found in the materials we use in our daily lives. They could be hydrogels, packaging materials and shape memory polymers and alloys. This constantly growing market requires new research on better and newer materials as soon as possible. Thus the need for skilled researchers is growing at a rapid pace.

I wish to thank all the contributing authors for sharing their expertise with us in this book. I also wish to thank them for submitting their contributions within the time frame set for this publication. I also wish to acknowledge the publishing team who worked tirelessly with me and assisted me throughout the editing process. Lastly, I wish to pay my regards to my friends and family who have always supported me.

Editor

Contents

Synthesis, Structural, and Electrical Properties of Pure $PbTiO_3$ Ferroelectric Ceramics

Vijendra A. Chaudhari[1] and Govind K. Bichile[2]

[1] *Department of Physics, Dayanand Science College, Latur 413 531, India*
[2] *Department of Physics, Dr. Babasaheb Ambedkar Marathwada University, Aurangabad 431 004, India*

Correspondence should be addressed to Vijendra A. Chaudhari; vijendra333@gmail.com

Academic Editor: Li Tao

Single-phase polycrystalline samples of lead titanate with perovskite structure have been synthesized using solid-state reaction technique. The processing parameters have been optimized to obtain phase pure, dense, crack-free, and homogeneous samples. The sintering behavior of PT-powders has been investigated using X-ray diffraction patterns. The X-ray powder diffraction data have been analyzed to confirm the phase formation and phase purity, to obtain unit cell parameters and unit cell volume. The porosity of the samples has been obtained through X-ray density and bulk density. The average particle sizes of the phase pure samples were obtained from the X-ray peak width using Scherrer's formula. The influence of sintering temperature and time on the microstructure of samples has also been studied by carrying out SEM investigations. The notable feature of this microstructure study shows that the samples sintered at 900°C for 12 hours possess a fairly uniform grain distribution. The electrical behavior (complex impedance Z^*, complex permittivity ε^*, etc.) of the samples sintered at 900°C for 12 hours has been studied by complex impedance spectroscopy. The temperature variation of real permittivity gives evidence of the ferroelectric phase transition as well as of the relaxation behavior.

1. Introduction

Crystals of the perovskitefamily, such as $PbTiO_3$, $BaTiO_3$, $SrTiO_3$ and, have been of constant interest because some ofthese materials show ferroelectric behavior and undergo structural phase transitions [1]. $PbTiO_3$ has been considered to be one of the most important members of this family. It has a high Curie temperature, high pyroelectric coefficient, low dielectric constant, and high spontaneous polarization [2]. Lead titanate ($PbTiO_3$, PT) is a ferroelectric ceramic that has not been proved to be a technologically important material by itself but is a significant component material in electronics such as capacitors, ultrasonic transducers, thermistors, and optoelectronics [3–7]. It is also a promising material for pyroelectric infrared detector applications because of its large pyroelectric coefficient and relatively low permittivity [8, 9]. $PbTiO_3$ (PT) has also been extensively used in a range of piezoelectric applications, as well as being the end member of technologically significant ferroelectric perovskite series such as $PbZr_{(x)}Ti_{(1-x)}O_3$ (PZT), $Pb_{(x)}Ca_{(1-x)}TiO_3$, $Pb(Zn_{1/3}Nb_{2/3})O_3$-(x) $PbTiO_3$ (PZN-PT), and Pb $(Mg_{1/3}Nb_{2/3})$ O_3-(x) $PbTiO_3$ (PMN-PT) and so forth. At ambient temperature, the material has a strong anisotropy which develops during cooling through the cubic-tetragonal phase transition of approximately 490°C. The anisotropy as measured by the tetragonality of the unit cell, c/a, may be as high as ~1.06. A large c/a ratio is considered favorable for enhanced electrical properties [10, 11].

The conventional method of synthesizing $PbTiO_3$ relies on the solid-state reaction between TiO_2 and $PbCO_3$ at high temperature. The conventional solid-state reaction has a tendency to produce a coarse $PbTiO_3$ powder with compositional inhomogeneity and a degree of particle agglomeration if the processing parameters are not carefully optimized. Therefore, many chemistry-based processing routes, including coprecipitation [12], sol-gel synthesis [13], hydrothermal [14], and citrate routes [15], have been devised for

the preparation of an ultrafine, sintering-reactive $PbTiO_3$ powder. However, almost all these chemistry routes require calcination of the precursors at an elevated temperature to develop the desired $PbTiO_3$ phase. Furthermore, most of these chemistry-based processing routes require high-purity inorganic or organometallic chemicals as the starting materials, which are many times more expensive than the widely available oxides and carbonates. It has been observed that the synthesis of a mechanically robust, high density, monolithic ceramic pure $PbTiO_3$ is not simple [16]. Problems typically encountered include loss of lead (Pb) due to the volatility of PbO at elevated temperatures, porosity, and microcracking, in extreme cases leading to spontaneous fracture. The main hurdle in the PT fabrication is the synthesis of a single phase with required perovskite structure. The primary difficulty is due to the volatility of PbO at elevated temperatures. The $PbTiO_3$ structure can only tolerate minor loss of lead (Pb), higher levels of which effectively promote second phase formation and the degradation of piezoelectric properties. An example is the formation of a PT phase with the pyrochlore structure observed during a coprecipitation synthesis experiment [12]. A more common occurrence is the formation of a two-phase mixture with TiO_2 [17]. The volatilization of PbO is known to increase markedly at temperatures above 800°C though the critical temperature is debated. Kim et al. [18] have observed that a PbO-rich PT in liquid phase is formed above 838°C, Algueró et al. [19] found that at 650°C an excess of 20% PbO was required because of Pb-loss during thermal treatments of sol-gel prepared La-modified PT thin films, whereas Ananta and Thomas [20] found that Pb volatility in PMN-PT could be minimized by careful sintering up to 1250°C. What is clear is that the loss of lead depends on particle size of constituent oxides, processing conditions, and chemical stability. The degree of Pb incorporation into the presintered crystal structure affects the volatility enormously [17]. Many groups report that loss of lead (Pb) may be minimized by sintering compacted powders in a surrounding lead-based powder or a PbO vapor atmosphere [18, 21] although this may lead to a Pb gradient in the final sintered product [17]. The problem of porosity has largely been addressed through particle size control of the starting powder. Therefore, one of the aim of the present work is to optimize the processing parameters to obtain homogeneous, dense, crack-free samples using the conventional solid-state reaction method. A careful and systematic study optimization of the synthesis parameters provides an alternative means of minimizing the problem of cracking, porosity, and Pb volatility. Careful sintering at lower temperatures may restrict grain growth and on cooling internal strains are reduced. In addition, sintering at low temperatures, the problem of volatility of lead is minimized. It has been shown that homogenous powders with a fine grain size can be produced by the ceramic process on the optimization of synthesis parameters [22]. The electrical properties result from the different contributions made from various components and processes present in the material, and complex impedance spectroscopy has been commonly used to evaluate and separate the contribution of the overall electrical properties in the frequency domain due to electrode reactions at the electrode/sample interface and migration of ions through the grains and across the grain boundaries in a polycrystalline material. In view of this, we report our studies on electrical properties of PT samples using complex impedance spectroscopy technique. The frequency dependent properties of a material can be described via the complex permittivity (ε^*), complex impedance (Z^*), and dielectric loss or dissipation factor ($\tan\delta$). These complex parameters are interrelated to one another as follows:

$$Z^* = Z' - jZ'' = \frac{1}{j\omega C_0 \varepsilon^*}, \tag{1}$$

$$\varepsilon^* = \varepsilon' - j\varepsilon'', \tag{2}$$

$$\varepsilon' = -\frac{Z''}{\omega C_0 \left(Z'^2 + Z''^2\right)}, \tag{3}$$

$$\varepsilon'' = \frac{Z'}{\omega C_0 \left(Z'^2 + Z''^2\right)}, \tag{4}$$

$$\tan\delta = \frac{\varepsilon''}{\varepsilon'} = \frac{Z'}{Z''}, \tag{5}$$

where $\omega = 2\pi f$ is the angular frequency, C_o is the geometrical capacitance, and $j = \sqrt{-1}$. The peak of the semicircle in the complex plane plot enables us to evaluate the relaxation frequency (f_{max}) of the bulk material in accordance with the relation

$$\begin{aligned} \omega\tau &= 1, \\ (2\pi f)\left(R_b C_b\right) &= 1, \\ f &= \frac{1}{2\pi R_b C_b}, \end{aligned} \tag{6}$$

where R_b and C_b are the bulk resistance and capacitance, and f is the relaxation frequency. Relaxation frequency and relaxation time (τ) depend on the intrinsic properties of the material and not on the sample geometrical factors. The term intrinsic properties of the material referred to the properties attributed to structure/microstructure (i.e., grain interior or bulk, grain boundary, etc.). These properties govern the distribution of resistive and capacitive components in the material on which the relaxation time ultimately depends. In short, here we have made an attempt to optimize the synthesis parameters and further study the structural, microstructural, and electrical properties of the PT compound.

In this paper, we have investigated the effect of processing parameters and optimized them to obtain single-phase, crack-free samples. The sintering behavior of the powders at various temperatures has been investigated using X-ray diffraction (XRD) patterns and scanning electron microscopy. The electrical behavior (complex impedance, complex permittivity, etc.) has been studied by complex impedance spectroscopy. The temperature and frequency variation of the electrical properties has also been investigated.

2. Experimental Procedures

$PbTiO_3$ (PT) samples were prepared by solid-state reaction processing using high purity oxide and carbonate as the starting materials, involving several steps such as mixing, wet grinding, calcination, and sintering along with intermediate grinding at each stage. Calcination at temperatures ranging from 450 to 550°C was carried out to synthesize the PT compound before sintering at different temperatures. Commercially available $PbCO_3$ (99.9% purity; Aldrich Chemicals) and TiO_2 (99.9% purity; Loba Chemie were used as starting materials. In order to compensate the loss of PbO during the high temperature sintering, 5% by weight excess of PbO was added.The excess PbO helps to compensate for the lead evaporation during sintering process. The polycrystalline samples of $PbTiO_3$ were prepared using the previous high purity ingredient materials in the required stoichiometry, and the powders were wet-milled. The sieved fine powders were then calcined in the temperature range 450–550°C for 8 hrsders were again finely ground and sieved through a 75 μm. The sieved powders were pressed in to pellets using polyvinyl alcohol (PVA) as a binder. The PT powders were then cold pressed into pellets of diameter 10 mm and thickness 1-2 mm at a pressure of 50 MPa using an isostatic hydraulic press. The pellets were sintered at four different temperatures 700°C, 750°C, 800°C, and 900°C for 12 hr. The heating program was carried out using Carbolite programmable high temperature furnace with Eurotherm temperature controller. The phase structure of sintered specimens was investigated with X-ray diffraction.The X-ray diffraction data was collected over the scattering angle range $10^\circ \leq 2\theta \leq 80^\circ$ at 2θ step 0.02° using CuKα (λ = 1.5418 A) radiations recorded at room temperature using X-ray powder diffractometer (Xpert Pro-PAN Philips). The morphological studies of all the sintered samples were carried out by using scanning electron microscopy (SEM). Samples were examined using a JEOL JSM-6360 A analytical scanning electron microscopy operated at 15 kV. For determining the average particle size from full width at half maximum (FWHM) the intensity of Bragg peak (101) was used. The density of the PT ceramic was measured using single pan balance and Archimedes principle. For electrical characterization, the sintered disks (900°C, 12 hrs) of PT samples were polished to make both the faces flat and parallel and electroded with high-purity air-drying conducting silver paste. The impedance measurements were carried out using a computer-controlled impedance analyzer (HP 4192 A LF HEWLETT) over a wide range of temperature (33°C–560°C) and frequency (5 Hz–13 MHz) with an applied voltage of 1.3 V. Measurements provided the real and imaginary parts of the impedance and dielectric as frequency-dependent values.

3. Results and Discussion

3.1. Structural and Microstructural Characterization. X-ray diffraction patterns collected at room temperature for the samples sintered at 700°C, 750°C, 800°C, and 900°C are shown in Figure 1. All the observed peaks/reflections are indexed in tetragonal crystals systems on the basis of the best agreement between observed and calculated interplaner (d) values. The values of unit cell parameters (a, c) and axial ratio (c/a) and density are given in Table 1. The comparative behavior of the tetragonality and unit cell volume with sintering temperature is shown in Figure 2, and the density variation with sintering temperature is shown in Figure 3. Figure 3 shows the measured and X-ray density (ρ_m, ρ_x) as a function of a sintering temperature. A slight increase in density is observed as sintering temperature increases up to 900°C. However, a density jump occurs at 750°C, and almost dense ceramics are achieved thereafter. The results are shown in Figure 3.

Table 1: Unit cell parameters and c/a ratio of PT powder samples sintered at different temperatures.

Sintering temperature (°C)	a (Å)	c (Å)	c/a ratio	Density (X-ray) (g/cm^3)	
				ρ_x	ρ_m
700	3.9008	4.067	1.0426	6.91	6.09
750	3.9013	4.0673	1.0425	7.85	7.18
800	3.9032	4.0679	1.0422	7.91	7.35
900	3.9023	4.0657	1.0419	7.97	7.43

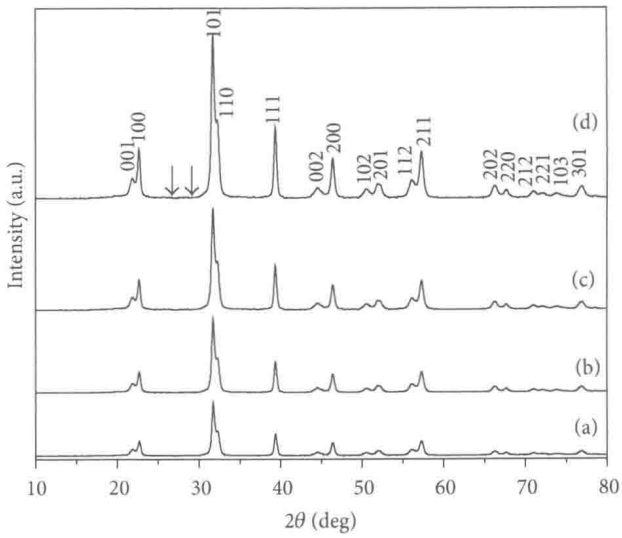

Figure 1: X-ray diffraction patterns of $PbTiO_3$ sample sintered at different temperatures ((a) = 700°C, (b) = 750°C, (c) = 800°C, and (d) = 900°C).

The powder diffraction peaks from sample sintered at different temperatures showed that all the samples possess single-phase perovskite structure. The diffraction peaks have narrowed substantially with the increasing sintering temperature and the PT phase has persisted without evidence of second phase formation. Sintering athigher temperatures does not appear to substantially alter the nature of patterns. However, the XRD pattern collected at the highest temperature 900°C, Figure 1(d), shows additional minor diffraction peaks, suggesting the beginning of the evolution of second phase (indicated by arrow). Figure 4 shows the XRD patterns for the samples that have been sintered at 900°C for various time periods (4, 8, and 12 hrs). Fine perovskite $PbTiO_3$ crystallites, as indicated by the peaks at 2θ angle of 21.8°, 22.5°, 31.6°,

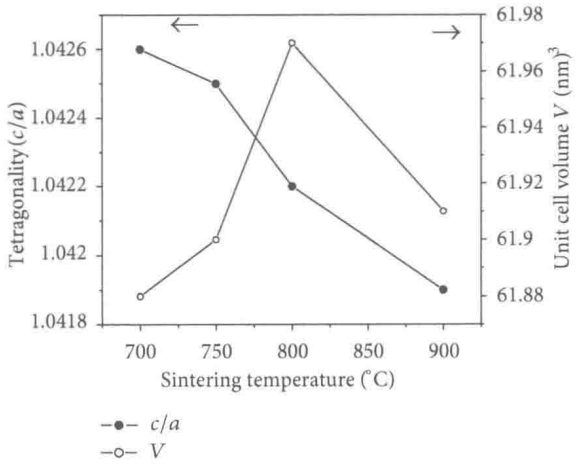

FIGURE 2: Variation of c/a and unit cell volume (V) with sintering temperature (°C).

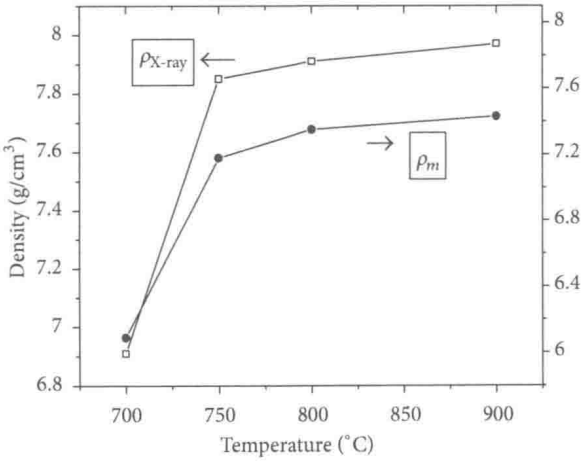

FIGURE 3: X-ray and measured density of the $PbTiO_3$ ceramics as a function of sintering temperature.

39.1°, 44.5°, 46.0°, 50.5°, 51.5°, 55.9°, and 56.9°, were observed, together with much weakened and broadened peaks of TiO_2 when the samples were subjected to for 4 hr sintering. This observation indicatesthat sintering at 900°C for the first 4 hrs triggers the formation of perovskites $PbTiO_3$ phase, and at the same time, the peak broadening of TiO_2 implies that the first sintering has led to a significant refinement in the particle and crystallite sizes. The $PbTiO_3$ phase was observed further when the sintering was extended to 8 hrs, which indicates that the formation of $PbTiO_3$ phase occurred at the expense of constituent oxides with increasing sintering time. $PbTiO_3$ was the only phase that was observed in the X-ray diffraction pattern in the sample that was sintered for 12 hrs The average particle size has been determined from the full width at half maximum (FWHM) of 101 peak using Scherrer's equation [23]

$$t = \frac{0.9\lambda}{B\cos\theta_B}, \tag{7}$$

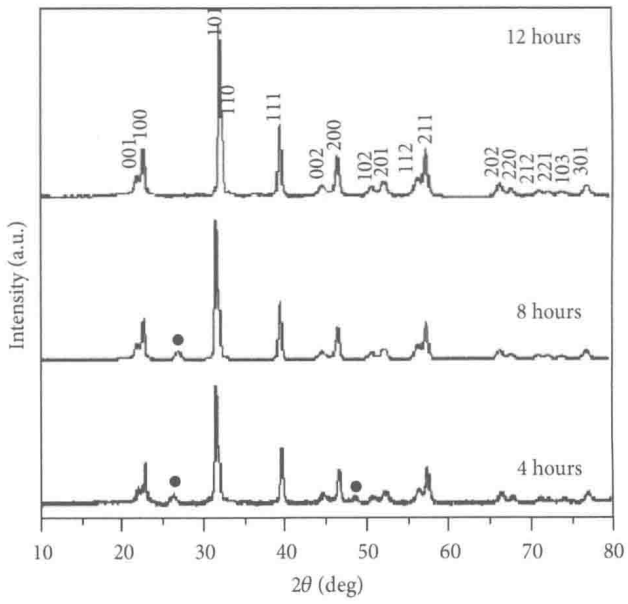

FIGURE 4: X-ray diffraction patterns of $PbTiO_3$ sample sintered at 900°C for various time durations (4, 8, and 12 hrs).

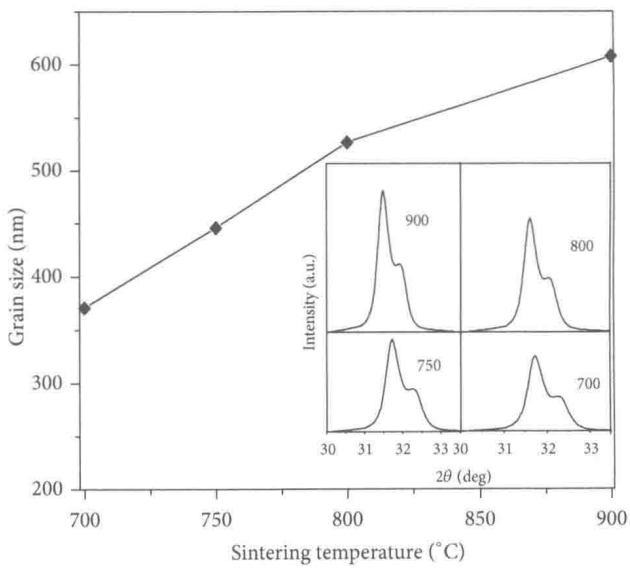

FIGURE 5: Particle sizes as a function of sintering temperatures. Figure in the inset shows the (101) peak. FWHM values were calculated from the Gaussian fits (solid lines).

where t is the particle diameter, λ the X-ray wavelength, B the FWHM of a diffraction peak, and θ_B the diffraction angle. The value of FWHM includes errors from the apparatus conditions such as the slit width of the X-ray diffractometer and these errors were corrected. The results were supported by the SEM micrograph studies. Figure 5 shows the variation of average particle sizes as a function of sintering temperatures determined from the peaks in the inset figures. Figure 6 shows the typical SEM pattern of $PbTiO_3$ sample sintered at 900°C for 12 hrs. The pattern shows that the $PbTiO_3$ particles have a more or less spherical morphology and consist of particle agglomerate of varying size, and the sizes of the grains

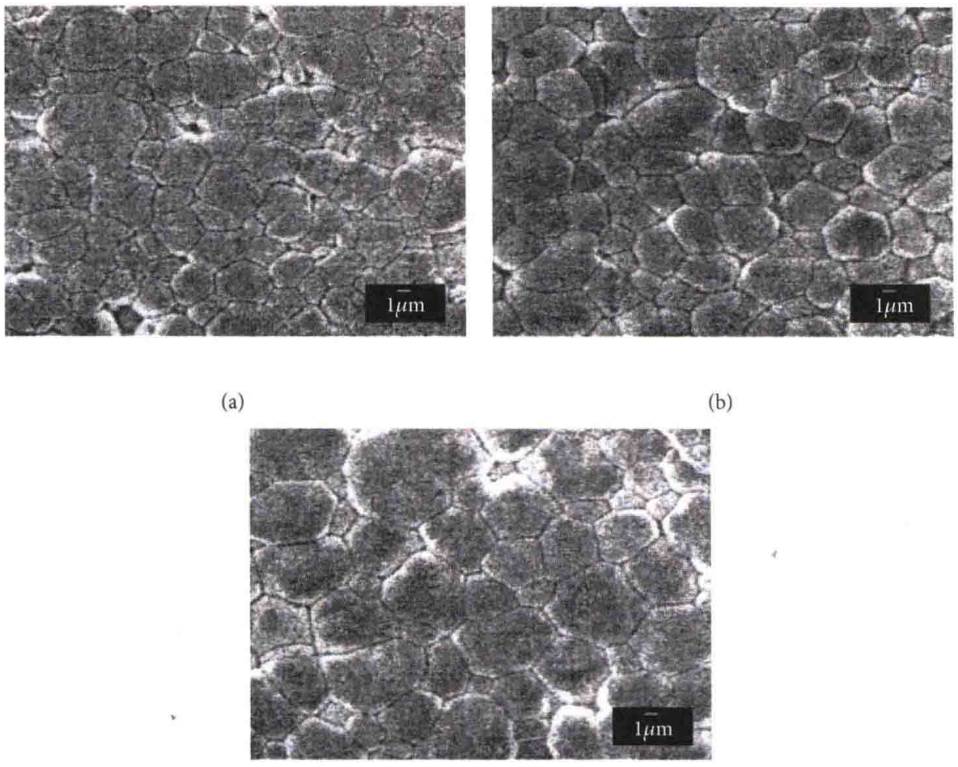

FIGURE 6: SEM micrograph for sample sintered at (a) = 750°C, (b) = 800°C, and (c) = 900°C for 12 hrs.

TABLE 2: Particle size (XRD), grain size (SEM) and phase and space group of $PbTiO_3$.

Sintering temperature (°C)	Particle size (nm)	SEM (nm)	Phase and space group
700	371	450	T (P4 mm)
750	446	540	T (P4 mm)
800	527	670	T (P4 mm)
900	608	883	T (P4 mm)

are in the range 500 to 600 nm. The particle size (XRD), grain size (SEM), and phase and space group are listed in Table 2.

3.2. Complex Impedance Study. Figure 7 shows the complex impedance spectrum of the PT compound at five different temperatures. From the nature of these plots, it is evident that the change in temperature ensures a distinct effect on the impedance spectrum of the material. The appearance of low temperature single circular arcs is due to the bulk properties of the material, and appearance of double arcs at high temperatures (inset Figure 7) is due to the consequence of bulk and grain boundary contribution to the conduction. These arcs appear in distinct frequency ranges, one at a higher frequency followed by another lower frequency arc. This feature is almost similar at different temperatures, also with a difference in radii of curvature of the arcs, which reduces with rise in temperature. The pattern in the impedance spectrum is a representative of the electrical processes taking place in the

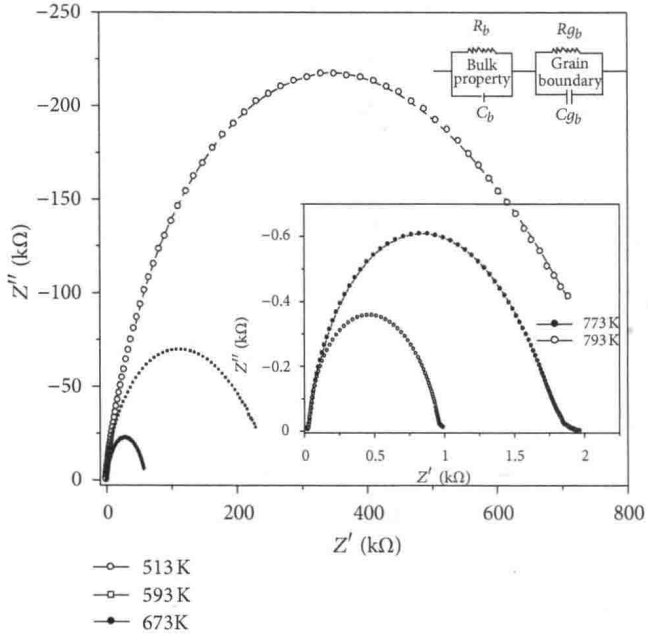

FIGURE 7: Nyquist plot of $PbTiO_3$ material at five different temperatures. Figure in the inset shows the equivalent electrical circuit.

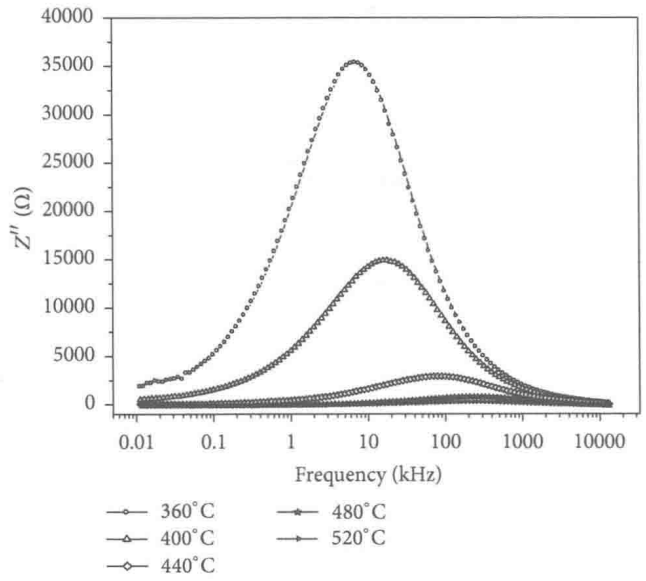

FIGURE 8: Frequency variation of imaginary impedance (Z'') of $PbTiO_3$ at different temperatures.

material which can be expressed as an equivalent electrical circuit comprising a parallel combination of resistive and capacitive elements. The presence of two arcs accordingly can be thought of as resulting from cascading effect of parallel combination of resistive and capacitive elements arising due to the contribution of bulk property of the material and grain boundary effect. The high frequency is attributed to the bulk property of the material (parallel combination of bulk resistance and bulk capacitance), and low frequency is due to the grain boundary effects in the material (parallel combination of grain boundary resistance and capacitance). The electrical processes taking place within the material have been modeled on for a polycrystalline system and are shown in terms of the equivalent electrical circuit in the Figure 7 (inset). Figure 8 shows the variation Z'' with frequency at different temperatures. The average peak position regularly shifts towards higher frequency as the temperature increases. This insures the temperature dependent relaxation process in the sample. Furthermore, as evident from the plots, as the temperature increases, the magnitude of Z'' decreases, the effect being more pronounced at the peak position. The shift of the peak towards higher frequency in raising the temperature is possibly due to the reduction in the bulk resistivity. The asymmetric peaks suggest the presence of electrical processes in the material with spread of relaxation time. The relaxation species may possibly be electrons or immobile species at lower temperature and defects at higher temperature that may be responsible for electrical conduction in the material.

Effectively large values of Z' and Z'' at low frequencies or temperatures indicate a predominant effect of the polarizations which consists of large ε values of PTs. The intercepts of the two semicircles are used to calculate the bulk resistance (R_b) and grain boundary resistance (R_{gb}) while the corresponding frequency values evaluated from the apex of the semicircles have been used to calculate the bulk and grain

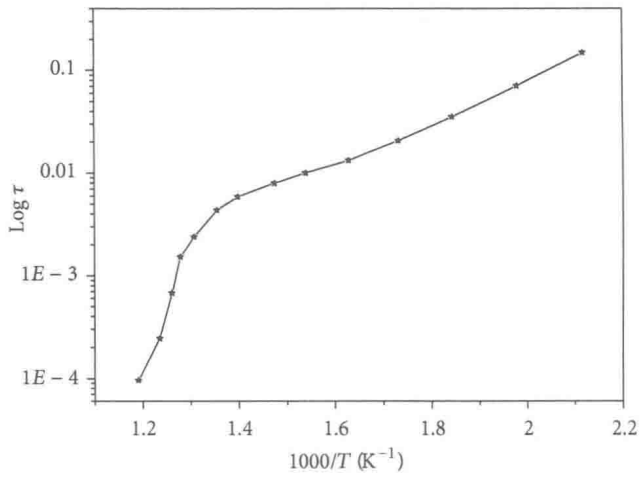

FIGURE 9: Plot of relaxation time with $10^3/T(K^{-1})$ of $PbTiO_3$.

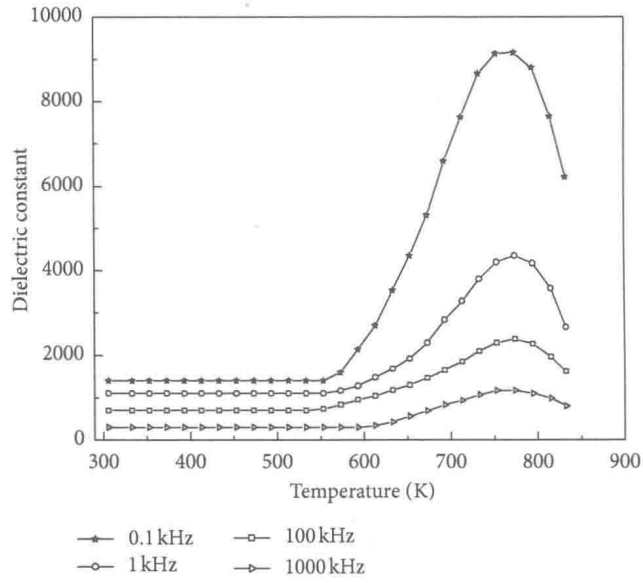

FIGURE 10: Temperature dependence of dielectric constant of $PbTiO_3$ at different frequencies.

boundary capacitance (C_b) using the relation, for a parallel combination of R and C

$$\omega_{max} C_b R_b = 1 \quad \text{or} \quad \omega_{max} C_{gb} R_{gb} = 1. \tag{8}$$

As temperature increases, both the grain resistance (R_b) and grain boundary resistance (R_{gb}) are found to decrease with rise in temperature indicated by a shift in the radius of the arcs towards left side on the real (Z') axis with increase in temperature. This provides convincing evidence that the electrical properties of PT are dependent on microstructure as well as temperature. A single nondegenarate process involves a single nondegenerate relaxation time for a given set of (R_b) and (C_b) at a temperature

$$\tau = C_b R_b = \frac{1}{\omega}. \tag{9}$$

The value of τ determined at selected temperatures in the region of measuring temperature using the values of (R_b) and

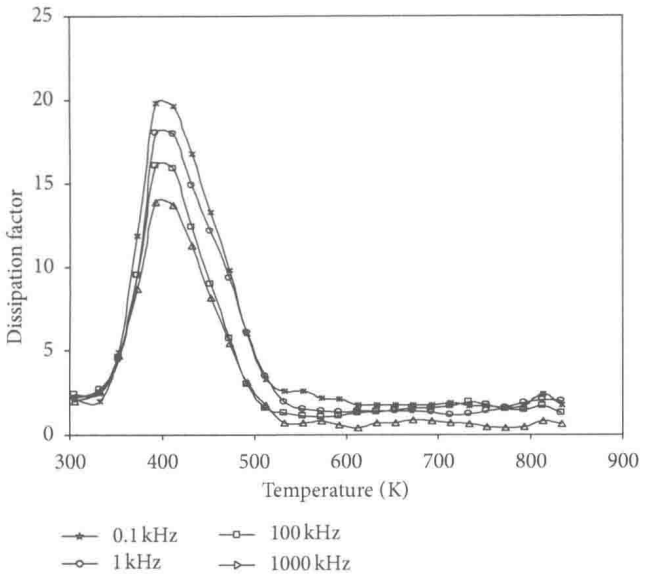

FIGURE 11: Temperature dependence of dissipation factor of $PbTiO_3$ at different frequencies.

TABLE 3: Relaxation time calculated from impedance data for $PbTiO_3$.

Temperature (°C)	R_g (Ω)	C_g (nF)	τ (s)
240	8.37×10^5	0.213	1.41×10^{-1}
320	2.47×10^5	0.202	3.42×10^{-2}
400	4.51×10^4	0.223	1.10×10^{-2}
440	9.87×10^3	0.204	5.92×10^{-3}
480	2.87×10^3	0.248	2.40×10^{-3}
500	2.00×10^3	0.316	1.53×10^{-3}
520	9.90×10^2	0.808	6.78×10^{-4}
540	6.44×10^2	0.554	2.46×10^{-4}

(C_b) in (9) is listed in Table 3. The τ-value is found to be decreasing linearly on increasing value of the temperature (~ above 600 K) suggesting a typical semiconductor behavior. The variation of τ with temperature (Figure 9) implies that the relaxation process is temperature dependent. The activation energy E_a evaluated from the slope of the curve by the relation

$$\tau = \tau_0 e^{-E_a/kT}, \tag{10}$$

where τ_0 is preexponential factor, E_a activation energy, k the Boltzmann constant and T the absolute temperature, is found to be 0.43 eV below 600 K and 2.1 eV above 600 K.

3.3. Complex Permittivity Study. The variation of real permittivity with temperature is shown in Figure 10. It is observed that the temperature dependence of real dielectric constant (ε') at different frequencies has typical features of relaxor ferroelectric. (i) the value of ε' increases gradually with rise in temperature and reaches a maximum value ε'_{max} at a particular temperature known as Curie temperature (T_c). This general feature is similar at all frequencies. (ii) The value of ε'_{max} at T_c decreases with increasing frequency. Further its value is larger at lower frequency (0.1 kHz). (iii) The value of T_c shifts towards the higher temperature side with increases in frequency. (iv) The Dielectric dispersion is absent at high temperatures beyond T_c whereas the dielectric constant has been observed to decrease with increasing frequencies at temperatures around and lower than T_c. This indicates strong dielectric dispersion at temperatures around and below T_c. The T_c value shifts from 750 to 850 K with the increased frequency value 0.1 kHz to 1000 kHz.

Figure 11 shows tan (δ) versus temperature (K) for $PbTiO_3$ at different frequencies. Dispersion in dielectric loss and shifting of dielectric loss peaks towards higher temperature side were observed with increase of frequency.

For a normal ferroelectric above the Curie temperature, the dielectric constant follows the Curie-Weiss law:

$$\varepsilon = \frac{c}{T - T_0}, \tag{11}$$

where c is the Curie constant and T_0 is the Curie-Weiss temperature [24–26]. For a ferroelectric with a diffuse phase transition (broad peak), the following equation:

$$\frac{1}{\varepsilon} = (T - T_m)^2 \tag{12}$$

has been shown to be valid over a wide temperature range instead of the normal Curie-Weiss law (11) [27, 28]. In (2), T_m is the temperature at which the dielectric constant is maximum. The degree of disorderness was evaluated using the relation [28, 29]

$$\frac{1}{\varepsilon} = \frac{1}{\varepsilon_{max}} + \frac{(T - T_{max})^\gamma}{2\varepsilon_{max}\delta^2}, \tag{13}$$

where ε_{max} is the maximum permittivity, γ the diffusivity, and δ is diffuseness parameter. The quantitative assessment of the diffusivity (γ) of the broadened peaks in the paraelectric phase was evaluated using the expression [30]

$$\ln\left(\frac{1}{\varepsilon} - \frac{1}{\varepsilon_{max}}\right) \text{ versus } (T - T_c)^\gamma. \tag{14}$$

The plot (Figure 12) of $\ln(1/\varepsilon - 1/\varepsilon_{max})$ versus $\ln(T - T_c)$ for all frequencies was use to obtain the values of γ. For value of $\gamma = 1$, the material exhibits Curie-Weiss behavior and for $\gamma = 2$, it is completely disordered. The value of γ lies between 1 to 2 and this confirm the diffuse phase transition. Table 4 gives the value of dielectric parameters for different frequencies.

4. Conclusions

The following interesting trends were revealed in the present study.

The unit cell dimensions are not significantly influenced by the sintering temperature. The *c/a* ratio does not vary significantly with sintering temperature, and its value is nearly 1.04. Gaussian's FWHM values are all small suggesting that the interparticle strains may contribute little to the

TABLE 4: Dielectric parameters of $PbTiO_3$ with different frequencies.

Frequency (kHz)	ε_{RT}	Tan δ_{RT}	T_c (°C)	ε_{max}	tan δ at T_c	γ
0.1	1400	2.10	480	9140	1.78	1.84
1	1100	2.20	490	4200	1.63	1.65
100	700	2.40	496	2300	1.56	1.68
1000	300	2.00	510	1170	0.51	1.80

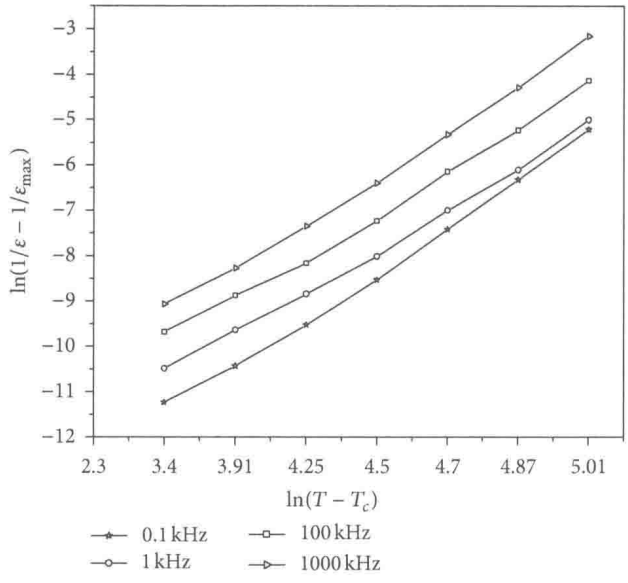

FIGURE 12: Plots of $\ln(1/\varepsilon - 1/\varepsilon_{max})$ versus $\ln(T - T_c)$ for $PbTiO_3$ ceramics at different frequencies.

diffraction peak shapes in these samples. The SEM micrographs do not exhibit the fracture surfaces of sample sintered at 900°C, and the sample has developed a relative uniform microstructure. $PbTiO_3$ powder can be synthesized directly from the constituent oxide using conventional ceramic technique by optimizing sintering temperature and time and by using starting oxides having fine uniform particle size. There is strong corelation between the crystallite sizes on the sintering temperature and supporting to the notion that crystallite size determines the propensity of microcracking. The *c/a* ratio does not differ much for the samples sintered at different temperatures. The experimental results on electrical properties indicate that the material exhibits conduction due to bulk and grain boundary effect at high temperature. The nature of loss spectrum (Figure 8) shows that the peaks shift towards the high frequency side with increase in temperature indicating relaxation process in the system. The broadening of the peaks on increasing temperature suggests the presence of temperature-dependant relaxation process in the system.

Acknowledgments

One of the author (V. A. Chaudhari) is thankful to Professor K.M. Jadhav Head of the Department of Physics, Dr. Babasaheb Ambedkar Marathwada University, Aurangabad, and Professor P. B. Joshi, B.C.U.D. Solapur University, for providing experimental facilities and helpful discussions.

References

[1] F. Jona and G. Shirane, *Ferroelectric Crystals*, MacMillan, New York, NY, USA, 1962.

[2] R. Migoni, H. Bilz, and D. Bauerle, "Origin of raman scattering and ferroelectricity in oxidic perovskites," *Physical Review Letters*, vol. 37, no. 17, pp. 1155–1158, 1976.

[3] L. E. Cross, "Dielectric, piezoelectric and ferroelectric components," *The Bulletin of the American Ceramic Society*, vol. 63, pp. 586–590, 1984.

[4] K. Sasazawa, K. Oshima, and N. Yamaoka, "Surface potential decay and residual voltage measurements in highly elongated polyethylene," *Japanese Journal of Applied Physics*, vol. 26, pp. L65–L67, 1987.

[5] T. R. Shrout and A. Halliyal, "Preparation of lead-based ferroelectric relaxors for capacitors," *American Ceramic Society Bulletin*, vol. 66, pp. 704–711, 1987.

[6] D. Damjanovic, T. R. Gururaja, and L. E. Cross, "Anisotropy in piezoelectric properties of modified lead titanate ceramics," *American Ceramic Society Bulletin*, vol. 66, no. 4, pp. 699–703, 1987.

[7] M. Kuwabara, "Lead titanate ceramics with positive temperature coefficients of resistivity," *Journal of the American Ceramic Society*, vol. 73, no. 5, pp. 1438–1439, 1990.

[8] Y. Chan, H. L. W. Chan, and C. L. Choy, "Nanocrystalline lead titanate and lead titanate/vinylidene fluoride-trifluoroethylene 0-3 nanocomposites," *Journal of the American Ceramic Society*, vol. 81, no. 5, p. 1231, 1998.

[9] R. Y. Ting, "Evaluation of new piezoelectric composite materials for hydrophone applications," *Ferroelectrics*, vol. 67, no. 1, pp. 143–157, 1978.

[10] G. Shirane and S. Hoshino, "On the phase transition in lead titanate," *Journal of the Physical Society of Japan*, vol. 6, pp. 265–270, 1951.

[11] Y. XU, *Ferroelectric Materials and Their Applications*, North Holland, Amsterdam, The Netherlands, 1991.

[12] L. B. Archer, C. D. Chandler, R. Kingsborough, and M. J. Hampden-Smith, "Synthesis and characterization of perovskite-phase mixed-metal oxides: lead titanate," *Journal of Materials Chemistry*, vol. 5, no. 1, pp. 151–158, 1995.

[13] T. W. Dekleva, J. M. Hayes, L. E. Cross, and G. L. Geoffroy, "Sol—gel processing of lead titanate in 2-methoxyethanol: investigations into the nature of the prehydrolyzed solutions," *Journal of the American Ceramic Society*, vol. 71, no. 5, pp. C280–C282, 1988.

[14] J. Moon, T. Li, C. A. Randall, and J. H. Adair, "Low temperature synthesis of lead titanate by a hydrothermal method," *Journal of Materials Research*, vol. 12, no. 1, pp. 189–197, 1997.

[15] J. D. Tsay and T. T. Fang, "Effects of temperature and atmosphere on the formation mechanism of barium titanate using the citrate process," *Journal of the American Ceramic Society*, vol. 79, no. 6, pp. 1693–1696, 1996.

[16] J. S. Forrester, J. S. Zobec, D. Phelan, and E. H. Kisi, "Synthesis of $PbTiO_3$ ceramics using mechanical alloying and solid state sintering," *Journal of Solid State Chemistry*, vol. 177, no. 10, pp. 3553–3559, 2004.

[17] L. S. Hong and C. C. Wei, "Effect of oxygen pressure upon composition variation during chemical vapor deposition growth of lead titanate films from tetraethyl lead and titanium tetraisopropoxide," *Materials Letters*, vol. 46, no. 2-3, pp. 149–153, 2000.